ACS Photonics

pubs.acs.org/journal/apchd5

Article

Silicon–Lithium Niobate Hybrid Intensity and Coherent Modulators Using a Periodic Capacitively Loaded Traveling-Wave Electrode

Zong Wang, Gengxin Chen, Ziliang Ruan, Ranfeng Gan, Pucheng Huang, Zhiwen Zheng, Liwang Lu, Jun Li, Changjian Guo, Kaixuan Chen,* and Liu Liu*

Cite This: *ACS Photonics* 2022, 9, 2668–2675

Read Online

ACCESS | Metrics & More | Article Recommendations | Supporting Information

Downloaded via NANJING UNIV on September 18, 2022 at 14:03:13 (UTC).
See https://pubs.acs.org/sharingguidelines for options on how to legitimately share published articles.

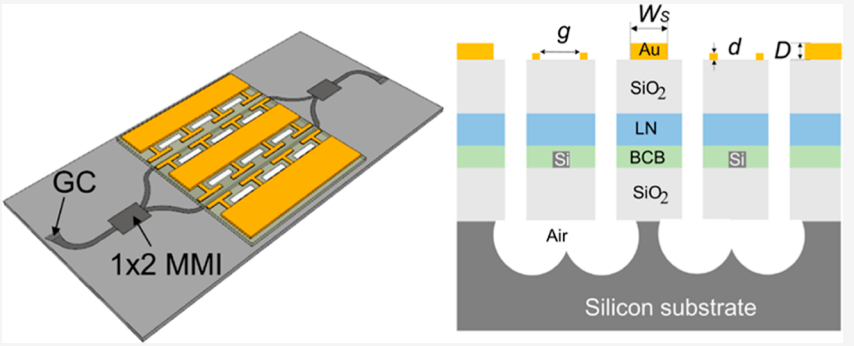

ABSTRACT: High-performance silicon and thin-film lithium niobate hybrid electro-optic modulators are demonstrated. In order to break the voltage–bandwidth limit in a normal traveling-wave modulator, a periodic capacitively loaded traveling-wave electrode is employed in this hybrid platform. The silicon substrate is undercut-etched to achieve index matching of the optical wave and microwave. A hybrid waveguide with a lithium niobate thin film bonded on a silicon wire is employed. Lithium niobate etching is not required for making the hybrid optical waveguides. We realize an intensity modulator of 12.5 mm long modulation section, which exhibits a low half-wave voltage of 1.7 V and a large 3 dB modulation bandwidth of >70 GHz. Data transmissions with various modulation formats beyond 100 Gbit/s are successfully achieved with dynamic extinction ratios of >8 dB. Combining the advantages of the silicon and thin-film lithium niobate platforms, a compact dual polarization coherent modulator is also experimentally demonstrated, on which 96 Gbaud 16-level quadrature amplitude modulation signals in both polarizations are successfully transmitted.

KEYWORDS: *hybrid integration, lithium niobate, silicon photonics, electro-optic modulator, coherent modulator*

INTRODUCTION

During the last two decades, silicon photonics has been developed as a promising platform for high-density and high-speed data transmission circuits. Due to its abilities for large-scale integration, low cost, and complementary metal oxide semiconductor compatibility, silicon photonics draws great interest from both academia and industry. High-performance devices and circuits have been demonstrated through monolithic or hybrid integrations on silicon, such as ultra-low loss waveguides and fiber interfaces,[1,2] multiplexers for various domains,[3,4] lasers and amplifiers,[5,6] photo-detectors (PDs),[7,8] and modulators,[9,10] as well as demo chips for high-speed data center interconnects and long-haul communications.[11,12] Among them, modulators and PDs are key components, whose performances directly determine the data rate of an optical communication channel. Nowadays, PDs on silicon have already reached a bandwidth of 265 GHz and a quantum efficiency of >25%.[8] On the other hand, conventional Mach–Zehnder interferometer (MZI) based modulators on silicon, due to intrinsic material properties, still suffer from a low bandwidth (50–60 GHz), a high driving voltage (~7 V), and a high loss (5–6 dB).[13] Although resonant structures have been introduced to alleviate these problems, they also raise other constraints, such as narrow working wavelength ranges.[14,15] The search for a general purpose electro-optic (EO) modulator on silicon that can match the performance of a silicon-based PD continues to be an important topic of research. Hybrid integration technology brings other materials more suitable for light modulation, such as InP,[16,17] special polymers,[18,19] two-dimensional (2D) materials,[20,21] plasmonics,[22,23] germanium,[24] and thin-film lithium niobate

Received: February 18, 2022
Published: July 21, 2022

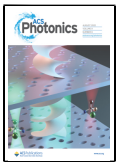

© 2022 American Chemical Society

https://doi.org/10.1021/acsphotonics.2c00263
ACS Photonics 2022, 9, 2668–2675

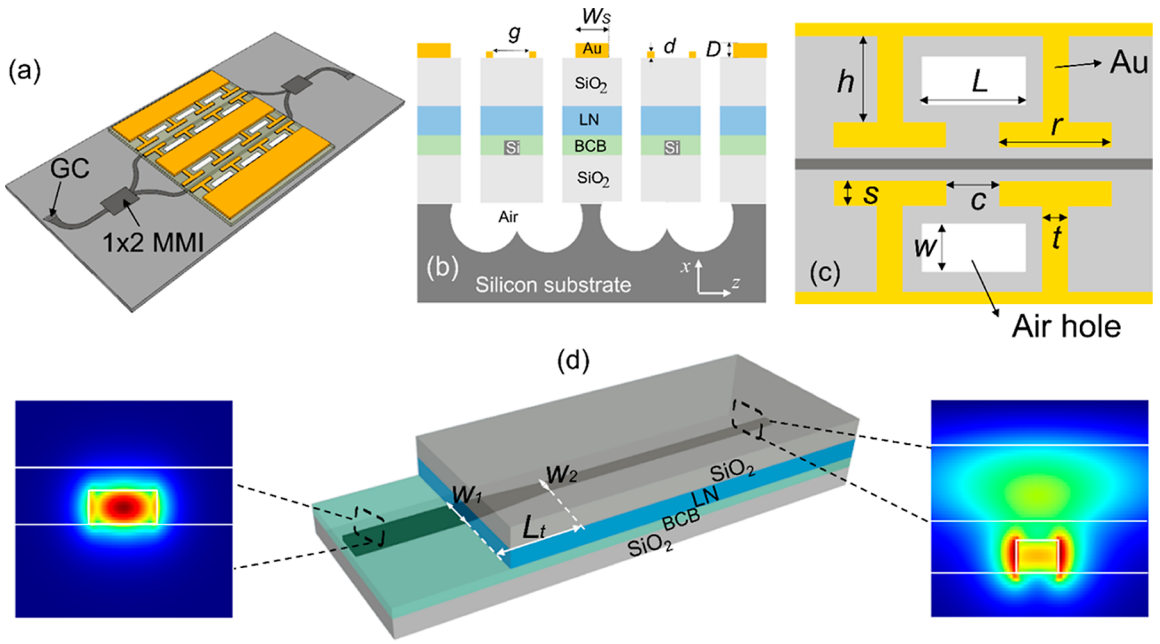

Figure 1. Proposed Si-TFLN hybrid modulator with a periodic CLTW electrode and an undercut etching in the silicon substrate. (a) Schematic of the MZI structure. (b) Cross-sectional view of the modulation section. (c) Detailed top view of the electrode structure. (d) Schematic of coupling section from a silicon wire waveguide to the hybrid waveguide. Insets show fundamental transverse electric mode profiles at corresponding positions.

(TFLN)[25−32] onto silicon, and have been envisioned as an effective approach to this goal. Among them, silicon−TFLN hybrid integration has been the most promising one, which enables to achieve modulation bandwidths of >70 GHz or half-wave voltages of <2 V, as well as low insertion losses.[26,29−32] However, such a silicon−TFLN hybrid modulator with a simultaneous large bandwidth and low driving voltage is still absent due to the intrinsic trade-off between these two figures using a traditional traveling-wave (TW) electrode.[33] For the same reason, the best silicon−TFLN hybrid modulator currently still used an etched ridge TFLN waveguide, where light is totally transferred into lithium niobate (LN) in the modulation section in order to maximize the light interaction with the EO material.

Recently, a periodic capacitively loaded TW (CLTW) electrode has been implemented to break such voltage−bandwidth limits on the monolithic TFLN platform.[34,35] The principle is that a wide signal electrode is used to reduce the radio frequency (RF) loss of the driving microwave signal, whereas the T-shaped periodic structures are added to maintain a small electrode gap for an efficient modulation. However, the microwave velocity in this case would be significantly reduced. A low-permittivity substrate, that is, quartz, had to be used to maintain the index matching between the optical and RF waves, which is not compatible with silicon photonics. In this paper, we demonstrate silicon−TFLN hybrid modulators with large bandwidths and low half-wave voltages using the CLTW electrode. The necessary index matching of the optical and RF waves is achieved through an undercut etching technique of the silicon substrate.[36] Additionally, a hybrid waveguide without etching LN is employed to facilitate the fabrication of the optical waveguide in the modulation section.[31] This structure avoids high-quality etching techniques to make smooth sidewalls of an LN ridge waveguide for a low propagation loss.[29] The fabricated 12.5 mm long intensity modulator exhibits a low V_π of 1.7 V and a large 3 dB EO bandwidth of >70 GHz. Based on the same hybrid platform, a highly integrated dual-polarization (DP) in-phase/quadrature (IQ) coherent modulator is also experimentally demonstrated. DP 16-level quadrature amplitude modulation (16QAM) signal at 96 Gbaud is successfully transmitted.

RESULTS

Device Design and Fabrication. Figure 1a shows the three-dimensional structure of the hybrid EO modulator on a silicon circuit. All the passive structures are built on a silicon-on-insulator (SOI) wafer of a 220 nm top silicon layer and a 2 μm buried oxide (BOX) layer. A pair of grating couplers (GCs) is used for the light in- and out-coupling to single-mode fibers. The intensity modulator essentially has an MZI structure, which includes two 1 × 2 multimode interferences on silicon and two hybrid-structured arms with a 500 nm thick x-cut TFLN bonded on the silicon waveguides. A layer of benzocyclobutene polymer with a thickness of 150 nm is used as the bonding layer between the TFLN and the top silicon layer. In each MZI arm, the light field transfers from the silicon wire waveguide to the hybrid waveguide adiabatically through a 300 μm long silicon taper and vice versa, as shown in Figure 1d. The width of the taper varies linearly from w_1 = 0.45 μm to w_2 = 0.28 μm. At w_1, the light is nearly all confined in the silicon wire, which ensures a low transition loss (>99.5%) from the input silicon circuit. On the other hand, at w_2 the light is more confined in the TFLN to ensure high modulation efficiency. The overall transmission loss of the taper structure is < 0.03 dB in simulation (details are provided in the Supporting Information).

The CLTW electrode is employed here to improve the modulation performances. In this structure, the wide signal electrode, that is, W_s = 65 μm, facilitates a low RF loss, whereas the T-shaped structures extending out from the main electrodes help maintain a strong electric field in the hybrid waveguide. In this case, the modulation efficiency, denoted as

https://doi.org/10.1021/acsphotonics.2c00263
ACS Photonics 2022, 9, 2668−2675

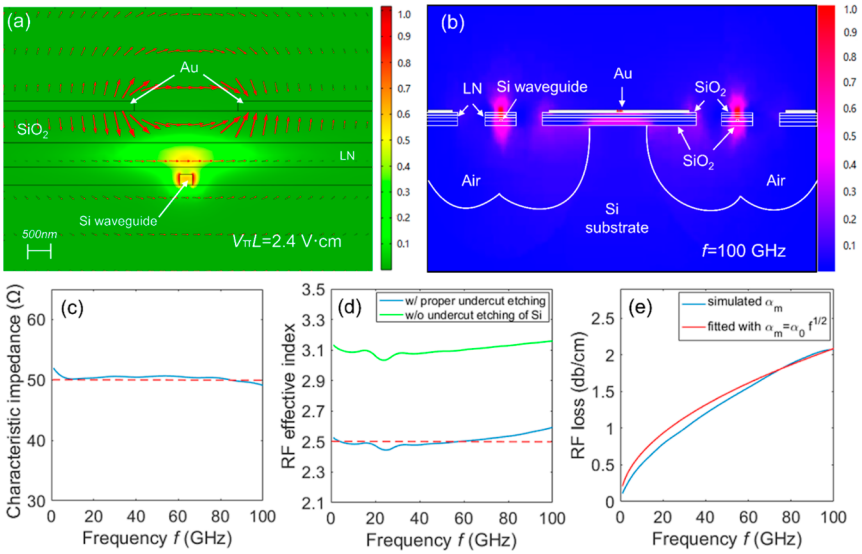

Figure 2. (a) Simulated optical mode profile (colormap) and static electrical field distribution (arrows) with an applied voltage of 30 V in the modulation region. (b) Simulated RF mode profile at a RF frequency of f = 100 GHz. Simulation results of (c) characteristic impedance, (d) RF effective index, and (e) RF loss α_m. The group index of the optical mode is marked as a red dash-dotted line in (d).

the half-wave voltage length product $V_\pi L$, and the modulation bandwidth can be improved simultaneously. Unfortunately, the RF velocity would be significantly reduced when using such an electrode structure. This causes a serious index mismatch between the optical and RF waves on a silicon substrate.[34] To solve this problem, the silicon substrate is undercut-etched for about 28 μm through the holes at the side of the hybrid waveguide in order to reduce the RF effective index and recover the necessary index matching, as shown in Figure 1b. The thickness d of the T structures is thin, 200 nm, considering its fine resolution, whereas the thickness D of the main electrodes is 1.1 μm to maintain a low RF loss. 650 nm thick silicon oxide over-cladding on the top of the TFLN is employed to isolate the electrode from the optical mode, so that the excessive light absorption loss induced by electrodes can be avoided (<0.025 dBcm^{-1}) even with a small gap of g = 2.28 μm and a structure misalignment of 0.25 μm resulted from fabrication. Other electrode parameters as noted in Figure 1c are carefully designed to ensure a good impedance and index matching required by a TW electrode, which gives (r, c, s, t, h, w, L) = (47, 3, 3, 5, 19, 13, 36) μm.

The electrical and optical mode properties in the modulation region were analyzed using a finite element algorithm (COMSOL) at 1550 nm wavelength as shown in Figure 2a,b. For the silicon wire of w_2 = 0.28 μm, the confinement factor in LN for the fundamental transverse electric mode is 58.2% (see the Supporting Information). This confinement factor is lower than that in an ordinary etched TFLN ridge waveguide,[37] which therefore gives a higher $V_\pi L$ of 2.4 V·cm in the present case. Nonetheless, as mentioned above the CLTW electrode design realized here effectively breaks the bandwidth−voltage limit of the modulator. A waveguide structure with relatively low light confinement in LN, such as the hybrid waveguide here, would only result in a longer device length without compromising the bandwidth. Using the optimized structural parameters, the characteristic impedance, the RF effective index, and the RF loss α_m obtained from simulations are shown in Figure 2c−e. The optical propagation loss induced by the metal electrodes is calculated to be about 0.07 dBcm^{-1}, which is negligible as compared to other loss mechanisms. One can find that the undercut etching technique indeed can help to achieve a nearly perfect index matching up to 100 GHz in this design. From Figure 2e, the frequency-independent characteristic RF loss α_0 can also be derived as 0.21 dBcm^{-1} GHz$^{-1/2}$, which is significantly lower than those of regular TW electrode-based Si−TFLN hybrid modulators.[28−32]

The fabrication of the proposed hybrid silicon and TFLN modulator consists of the SOI structure processing in a complementary metal oxide semiconductor fab, the die-to-die/wafer bonding of TFLN, the electrode metal patterning, and the undercut etching of the silicon substrate (details are included in the Supporting Information). Except for the initial SOI structures, all the other patterns in the proposed device are in the order of several microns and thus medium-resolution patterning tools, such as ultraviolet contact photo-lithography, can be used. Wafer-scale processing in the level of SOI wafer size is also possible if multi-die-to-wafer bonding of the TFLN should be adopted.

Performances of an Intensity Modulator. First, an MZI intensity modulator as shown in Figure 1a was fabricated. Figure 3a shows SEM images of the CLTW electrode and an optical image of the whole fabricated device. The length of the modulation section using the hybrid waveguide is 12.5 mm. The optical transmission of this device was then measured as shown in Figure 3b before the metal electrode deposition. Here, the input and output GC responses were normalized out. A typical MZI interference spectrum is presented due to the slight length difference in the SOI waveguides of the two arms. The measured insertion loss and extinction ratio of the modulator is 2 dB and 25 dB, respectively. The insertion loss here mainly comes from the propagation loss of the long modulation section, that is, the hybrid waveguide, which can be estimated as 1.6 dBcm^{-1} (the losses of the silicon multimode interferences and tapers are negligible). This is a typical value for the propagation loss of a silicon wire waveguide. Improving the processing for the silicon circuits would further decrease the insertion loss of the proposed modulator. After the whole device fabrication, the total insertion loss of the chip is 10.2 dB, including the coupling

https://doi.org/10.1021/acsphotonics.2c00263
ACS Photonics 2022, 9, 2668−2675

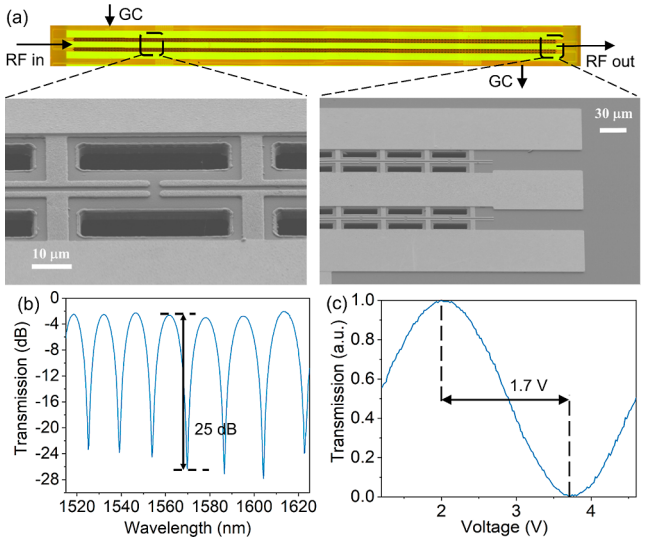

Figure 3. (a) Optical and SEM images of the fabricated device. (b) Transmission of the fabricated modulator before the electrode deposition. (c) Normalized optical transmission as a function of applied voltage showing a $V\pi$ of 1.7 V.

losses of two GCs to the fibers, that is, 7.2 dB. The insertion loss increased by 1 dB, which mainly comes from the metal electrodes, is more than expected from simulations. It can be attributed to the negative deviation of the over-cladding SiO_2 thickness and misalignment of the metal patterns resulted from the manual mask aligner. The modulation efficiency of this structure was further measured using a 100 kHz triangular-wave voltage drive. A typical sinusoidal response of the output optical signal was obtained as shown in Figure 3c. The half-wave voltage can then be extracted as V_π = 1.7 V. The corresponding $V_\pi L$ is 2.13 V·cm, which is also slightly smaller than the theoretical value. This also indicates that the over-cladding SiO_2 might be thinner than the desired 650 nm.

To characterize the bandwidth of the MZI modulator, the electrical−electrical (EE) performance of the CLTW electrode was first measured using a vector network analyzer, and the S_{12} and S_{11} responses is shown in Figure 4a. The 6.4 dB bandwidth of S_{21} clearly surpasses 67 GHz, and S_{11} is below −20 dB over the whole frequency range. For a TW modulator with perfect index and impedance matching, the 6.4 dB bandwidth of the EE response determines the 3 dB EO bandwidth of the modulator.[38] The deducted electrode parameters, including the characteristic impedance, the RF refractive index, and the RF loss, are illustrated in Figure 4b−d. The RF refractive index is slightly higher than the designed value, probably due to insufficient undercut etching of the silicon substrate. The characteristic RF loss α_0 fitted from Figure 4d is about 0.49 $dBcm^{-1}$ $GHz^{-1/2}$, which is also higher than the simulated results. The extra RF losses may be attributed to dielectric losses of the deposited oxide and scattering losses from the rough metal surfaces. Nevertheless, this loss value is still much lower than that of regular TW electrode-based Si−TFLN hybrid modulators.[28−32] The EO bandwidth of the modulator was further measured as shown in Figure 4e. A large EO bandwidth of >70 GHz is achieved thanks to the good index matching achieved from the undercut-etched structure here. The simulated EO response using the measured electrode parameters from Figure 4b−d predicts a 3 dB bandwidth of 100 GHz for the present device.

Data transmissions using the fabricated device were characterized using different modulation formats, including the on−off key (OOK), 4-level pulse amplitude modulation (PAM4), and 8-level pulse amplitude modulation (PAM8), as shown in Figure 5a. Clear eye opening can be observed up to 168 Gbit/s (56GBaud PAM8) data rate. In all the above eye measurements, the driving voltages were less than 2 V and the dynamic ERs are all better than 8 dB. The back-to-back (B2B) bit error rates (BERs) of 64 and 100 Gbit/s OOK signals were further measured and calculated using offline digital signal processing algorithms (details are included in the Supporting Information). As shown in Figure 5b, the BERs can drop below the KP-4 forward error correction threshold with a low received optical power, and no error floor is observed. Table 1 summarizes the key performances of some demonstrated EO intensity modulators on silicon or silicon hybrid platforms. One can find that the proposed device here shows better EO

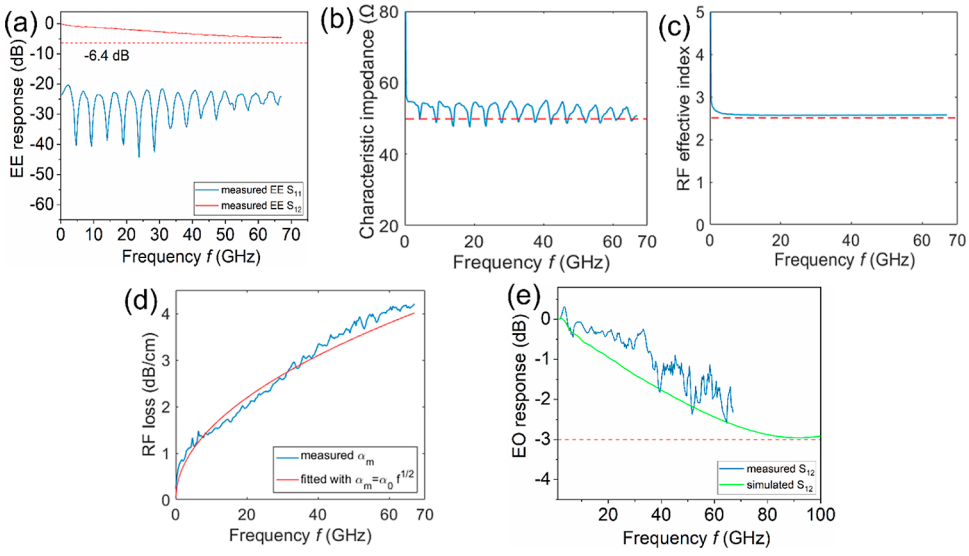

Figure 4. (a) Measured EE reflection S_{11} and transmission S_{12} of the device. Deduced (b) characteristic impedance, (c) RF effective index, and (d) RF loss. The red dash-dotted line in (c) indicates the optical group index. (e) Measured and simulated EO S_{21}.

https://doi.org/10.1021/acsphotonics.2c00263
ACS Photonics 2022, 9, 2668−2675

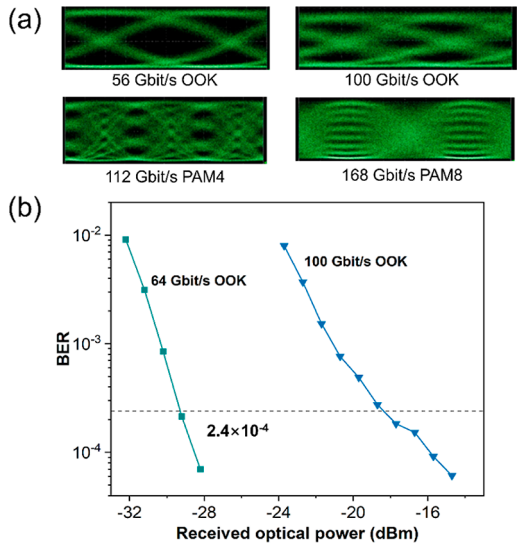

Figure 5. (a) Measured eye diagrams for 56 Gbit/s OOK, 100 Gbit/s OOK, 112 Gbit/s PAM4, and 168 Gbit/s PAM8 signals. (b) Measured B2B BERs for 64 Gbit/s and 100 Gbit/s OOK signals at different received optical power.

Table 1. Comparison of Several Performance Metrics for EO Modulators on Silicon at the C-Band

platform	loss (dB)	V_π (V)	EO bandwidth (GHz)	length (mm)
pure silicon[13]	5.4	7	58	2
Si–InP[16]	1	3.5	2.2	0.25
Si–polymers[19]	0.22	1.8	68	8
Si–graphene[20]	17	7	5	0.4
Si–plasmonics[22]	12	N/A	65	0.029
Si–TFLN[29]	2.5	5.1	70	5
Si–TFLN[30]	1.8	3	70	9
Si–TFLN[31]	7.6	13.4	>106	5
this work	3	1.7	>70	12.5

bandwidth with a smaller V_π, as compared to the other silicon–TFLN hybrid modulator using the conventional TW electrode.

Performances of a Coherent Modulator. To demonstrate the feasibility of the proposed hybrid modulator structure, which combines the advantages of silicon and TFLN platforms, for constructing complex circuits, a compact DP-IQ modulator for coherent communications was also fabricated. As shown in Figure 6a, the whole structure includes two 2D GCs for light input and polarization multiplexed output, four MZI modulators, on-chip 50 Ω termination resistors, and heaters for phase tuning. Except for the hybrid modulation sections, all the other components are on pure silicon, where high-performance 2D GCs with low coupling losses and low polarization-dependent losses,[1] and high-efficiency thermo-optic phase shifters[39] can be built. The final fabricated device is shown in Figure 6b,c. The length of modulation arms is 7.5 mm, corresponding to a measured V_π of 3 V and a bandwidth of also >70 GHz. Thanks to the compact silicon components, the size of the whole structure is only 9 mm × 1.6 mm. Modulation of a 96 Gbaud DP-16QAM signal using the present modulator and the corresponding coherent detection was experimentally demonstrated (detailed measurement procedures are provided in the Supporting Information). Clear constellations with signal-to-noise ratios of about 15 dB and BERs of better than 1×10^{-3} can be obtained for both polarizations as shown in Figure 6d.

CONCLUSIONS

We have demonstrated hybrid silicon and TFLN modulators using a CLTW electrode with undercut etching in the silicon substrate to break voltage–bandwidth limits of TW EO modulators in silicon photonics. The fabricated 12.5 mm long intensity modulator exhibits a low V_π of 1.7 V, a large 3 dB EO bandwidth of >70 GHz, and an insertion loss of 3 dB at the C-band. Data transmissions with OOK, PAM4, and PAM8 modulation formats beyond 100 Gbit/s have been successfully achieved. Thanks to the mature silicon passive components, a compact and high-performance coherent modulator with 96 Gbaud DP-16QAM data transmission was also experimentally demonstrated. In the present demonstration, good index and impedance matching has been achieved. Therefore, the EO bandwidth of the present modulator depends mainly on the RF losses of the electrode and increasing the length of the modulation section further could help achieve sub-one-volt driving voltage, which is essential for a driverless transmitter.

Apparently, the silicon–LN hybrid integration in this work takes advantages of excellent modulation performances on LN and matured compact devices on silicon, which are not simultaneously available on either single platform. The hybrid waveguide, using a TFLN bonded on a silicon wire waveguide,

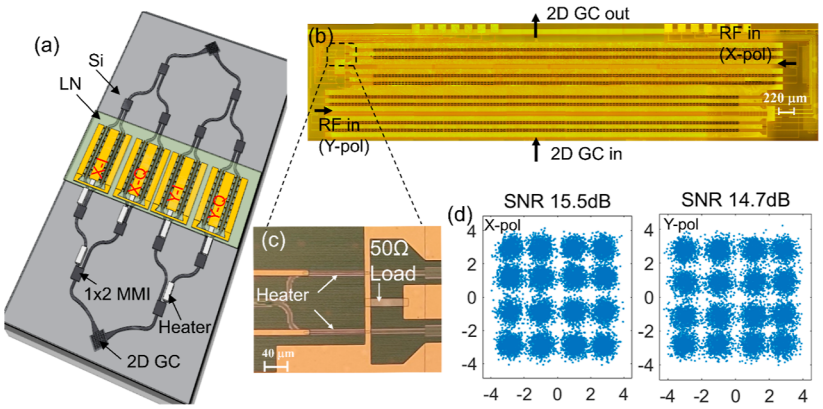

Figure 6. (a) Schematic of the DP-IQ modulator using the proposed Si–TFLN hybrid integration. (b) Microscope images of the whole modulator. (c) Zoom-in view of the on-chip 50 Ω resisters and heaters. (d) Measured DP-16QAM constellations.

https://doi.org/10.1021/acsphotonics.2c00263
ACS Photonics 2022, 9, 2668–2675

avoids specialized high-quality etching processes for LN structures with smooth sidewalls, which are currently not widely adopted. The fabrication processes for the hybrid modulator can also be integrated to an SOI wafer with, for example, germanium PDs, to enable a fully functional, high-performance photonic circuit on silicon. In this circumstance, the thick oxide over-cladding on the modulator area has to be removed to expose the silicon waveguide using, for example, dry etching. Fortunately, the benzocyclobutene adhesive layer used here facilitates the bonding on a relatively rough surface that resulted from the etching. One issue of the proposed device is related to the suspended structure, which appears to be unstable. Yet, the substrate undercut etching would be the last wafer processing step, and this structure also survived the mechanical dicing process in the test. Additionally, this type of suspended structure has also been widely adopted in micro-electromechanical systems, as well as silicon modulators.[13] We believe that the present demonstration of silicon−TFLN hybrid modulators would significantly improve the overall performance of integrated transceivers in silicon photonics platforms.

■ ASSOCIATED CONTENT

Supporting Information

The Supporting Information is available free of charge at https://pubs.acs.org/doi/10.1021/acsphotonics.2c00263.

Silicon−TFLN hybrid waveguide modeling; modulation efficiency modeling; fabrication process; and data transmission measurement (PDF)

■ AUTHOR INFORMATION

Corresponding Authors

Kaixuan Chen − *Guangdong Provincial Key Laboratory of Optical Information Materials and Technology, South China Academy of Advanced Optoelectronics, South China Normal University, Guangzhou 510006, China; National Center for International Research on Green Optoelectronics, South China Normal University, Guangzhou 510006, China*; Email: chenkaixuan@m.scnu.edu.cn

Liu Liu − *State Key Laboratory for Modern Optical Instrumentation, College of Optical Science and Engineering, International Research Center for Advanced Photonics, Zijingang Campus, Zhejiang University, Hangzhou 310058, China*; orcid.org/0000-0002-3651-544X; Email: liuliuopt@zju.edu.cn

Authors

Zong Wang − *Guangdong Provincial Key Laboratory of Optical Information Materials and Technology, South China Academy of Advanced Optoelectronics, South China Normal University, Guangzhou 510006, China*

Gengxin Chen − *State Key Laboratory for Modern Optical Instrumentation, College of Optical Science and Engineering, International Research Center for Advanced Photonics, Zijingang Campus, Zhejiang University, Hangzhou 310058, China*

Ziliang Ruan − *State Key Laboratory for Modern Optical Instrumentation, College of Optical Science and Engineering, International Research Center for Advanced Photonics, Zijingang Campus, Zhejiang University, Hangzhou 310058, China*

Ranfeng Gan − *Guangdong Provincial Key Laboratory of Optical Information Materials and Technology, South China Academy of Advanced Optoelectronics, South China Normal University, Guangzhou 510006, China*

Pucheng Huang − *Guangdong Provincial Key Laboratory of Optical Information Materials and Technology, South China Academy of Advanced Optoelectronics, South China Normal University, Guangzhou 510006, China*

Zhiwen Zheng − *Guangdong Provincial Key Laboratory of Optical Information Materials and Technology, South China Academy of Advanced Optoelectronics, South China Normal University, Guangzhou 510006, China*

Liwang Lu − *Guangdong Provincial Key Laboratory of Optical Information Materials and Technology, South China Academy of Advanced Optoelectronics, South China Normal University, Guangzhou 510006, China; National Center for International Research on Green Optoelectronics, South China Normal University, Guangzhou 510006, China*

Jun Li − *Guangdong Provincial Key Laboratory of Optical Information Materials and Technology, South China Academy of Advanced Optoelectronics, South China Normal University, Guangzhou 510006, China*

Changjian Guo − *Guangdong Provincial Key Laboratory of Optical Information Materials and Technology, South China Academy of Advanced Optoelectronics, South China Normal University, Guangzhou 510006, China; National Center for International Research on Green Optoelectronics, South China Normal University, Guangzhou 510006, China*

Complete contact information is available at: https://pubs.acs.org/10.1021/acsphotonics.2c00263

Funding

National Major Research and Development Program (2019YFB1803902); National Natural Science Foundation of China (NSFC) (62135012, 62105107); Leading Innovative and Entrepreneur Team Introduction Program of Zhejiang (2021R01001); Guangdong Basic and Applied Basic Research Foundation (2021A1515012215, 2021B1515120057); Science and Technology Planning Project of Guangdong Province (2019A050510039); and Fundamental Research Funds for the Central Universities (2021QNA5001).

Notes

The authors declare no competing financial interest.

■ REFERENCES

(1) Marchetti, R.; Lacava, C.; Carroll, L.; Gradkowski, K.; Minzioni, P. Coupling strategies for silicon photonics integrated chips. *Photonics Res.* **2019**, *7*, 201−239.

(2) Liu, L.; Zhang, J.; Zhang, C.; Wang, S.; Jin, C.; Chen, Y.; Chen, K.; Xiang, T.; Shi, Y. Silicon waveguide grating coupler for perfectly vertical fiber based on a tilted membrane structure. *Opt. Lett.* **2016**, *41*, 820−823.

(3) Chen, L.; Doerr, C. R.; Buhl, L.; Baeyens, Y.; Aroca, R. A. Monolithically integrated 40-wavelength demultiplexer and photodetector array on silicon. *IEEE Photonics Technol. Lett.* **2011**, *23*, 869−871.

(4) Chen, K.; Wang, S.; Chen, S.; Wang, S.; Zhang, C.; Dai, D.; Liu, L. Experimental demonstration of simultaneous mode and polarization-division multiplexing based on silicon densely packed waveguide array. *Opt. Lett.* **2015**, *40*, 4655−4658.

(5) Duan, G.-H.; Jany, C.; Le Liepvre, A.; Accard, A.; Lamponi, M.; Make, D.; Kaspar, P.; Levaufre, G.; Girard, N.; Lelarge, F. Hybrid III–V on Silicon Lasers for Photonic Integrated Circuits on Silicon. *IEEE J. Sel. Top. Quantum Electron.* **2014**, *20*, 158−170.

(6) Haq, B.; Kumari, S.; Van Gasse, K.; Zhang, J.; Gocalinska, A.; Pelucchi, E.; Corbett, B.; Roelkens, G. Micro-transfer-printed III-V-on-silicon C-band semiconductor optical amplifiers. *Laser Photonics Rev.* **2020**, *14*, 1900364.
(7) Koepfli, S. M.; Baumann, M.; Giger, S.; Keller, K.; Horst, Y.; Salamin, Y.; Fedoryshyn, Y.; Leuthold, J. High-speed graphene photodetection: 300 GHz is not the limit. *2021 Conference on Lasers and Electro-Optics Europe & European Quantum Electronics Conference (CLEO/Europe-EQEC)*; IEEE, 2021; p 1.
(8) Virot, L. Ultrafast on-chip germanium photodiode. *Nat. Photonics* **2021**, *15*, 868−869.
(9) Witzens, J. High-speed silicon photonics modulators. *Proc. IEEE Inst. Electr. Electron. Eng.* **2018**, *106*, 2158−2182.
(10) Li, K.; Liu, S.; Thomson, D. J.; Zhang, W.; Yan, X.; Meng, F.; Littlejohns, C. G.; Du, H.; Banakar, M.; Ebert, M.; Cao, W.; Tran, D.; Chen, B.; Shakoor, A.; Petropoulos, P.; Reed, G. T. Electronic−photonic convergence for silicon photonics transmitters beyond 100 Gbps on−off keying. *Optica* **2020**, *7*, 1514−1516.
(11) Fathololoumi, S.; Hui, D.; Jadhav, S.; Chen, J.; Nguyen, K.; Sakib, M.; Li, Z.; Mahalingam, H.; Amiralizadeh, S.; Tang, N. N.; Potluri, H.; Montazeri, M.; Frish, H.; Defrees, R. A.; Seibert, C.; Krichevsky, A.; Doylend, J. K.; Heck, J.; Venables, R.; Dahal, A.; Awujoola, A.; Vardapetyan, A.; Kaur, G.; Cen, M.; Kulkarni, V.; Islam, S. S.; Spreitzer, R. L.; Garag, S.; Alduino, A.; Chiou, R.; Kamyab, L.; Gupta, S.; Xie, B.; Appleton, R. S.; Hollingsworth, S.; McCargar, S.; Akulova, Y.; Brown, K. M.; Jones, R. J.; Zhu, D.; Liljeberg, T.; Liao, L. 1.6 Tbps silicon photonics integrated circuit and 800 Gbps photonic engine for switch co-packaging demonstration. *J. Lightwave Technol.* **2021**, *39*, 1155−1161.
(12) Zhang, H.; Li, M.; Zhang, Y.; Zhang, D.; Liao, Q.; He, J.; Hu, S.; Zhang, B.; Wang, L.; Xiao, X.; Qi, N.; Yu, S. 800 Gbit/s transmission over 1 km single-mode fiber using a four-channel silicon photonic transmitter. *Photonics Res.* **2020**, *8*, 1776−1782.
(13) Li, M.; Wang, L.; Li, X.; Xiao, X.; Yu, S. Silicon intensity Mach−Zehnder modulator for single lane 100 Gb/s applications. *Photonics Res.* **2018**, *6*, 109−116.
(14) Tong, Y.; Hu, Z.; Wu, X.; Liu, S.; Chang, L.; Netherton, A.; Chan, C.-K.; Bowers, J. E.; Tsang, H. K. An experimental demonstration of 160-Gbit/s PAM-4 using a silicon micro-ring modulator. *IEEE Photonics Technol. Lett.* **2019**, *32*, 125−128.
(15) Zheng, X.; Chang, E.; Amberg, P.; Shubin, I.; Lexau, J.; Liu, F.; Thacker, H.; Djordjevic, S. S.; Lin, S.; Luo, Y.; Yao, J.; Lee, J. H.; Raj, K.; Ho, R.; Cunningham, J. E.; Krishnamoorthy, A. V. A high-speed, tunable silicon photonic ring modulator integrated with ultra-efficient active wavelength control. *Opt. Express* **2014**, *22*, 12628−12633.
(16) Hiraki, T.; Aihara, T.; Hasebe, K.; Takeda, K.; Fujii, T.; Kakitsuka, T.; Tsuchizawa, T.; Fukuda, H.; Matsuo, S. Heterogeneously integrated iii−v/si mos capacitor mach−zehnder modulator. *Nat. Photonics* **2017**, *11*, 482−485.
(17) Han, J.-H.; Boeuf, F.; Fujikata, J.; Takahashi, S.; Takagi, S.; Takenaka, M. Efficient low-loss InGaAsP/Si hybrid MOS optical modulator. *Nat. Photonics* **2017**, *11*, 486−490.
(18) Kieninger, C.; Kutuvantavida, Y.; Elder, D. L.; Wolf, S.; Zwickel, H.; Blaicher, M.; Kemal, J. N.; Lauermann, M.; Randel, S.; Freude, W.; Dalton, L. R.; Koos, C. Ultra-high electro-optic activity demonstrated in a silicon-organic hybrid modulator. *Optica* **2018**, *5*, 739−748.
(19) Lu, G.-W.; Hong, J.; Qiu, F.; Spring, A. M.; Kashino, T.; Oshima, J.; Ozawa, M.-a.; Nawata, H.; Yokoyama, S. High-temperature-resistant silicon-polymer hybrid modulator operating at up to 200 Gbit/s for energy-efficient datacentres and harsh-environment applications. *Nat. Commun.* **2020**, *11*, 4224.
(20) Sorianello, V.; Contestabile, G.; Romagnoli, M. Graphene on silicon modulators. *J. Lightwave Technol.* **2020**, *38*, 2782−2789.
(21) Sorianello, V.; Midrio, M.; Contestabile, G.; Asselberghs, I.; Van Campenhout, J.; Huyghebaert, C.; Goykhman, I.; Ott, A.; Ferrari, A.; Romagnoli, M. Graphene−silicon phase modulators with gigahertz bandwidth. *Nat. Photonics* **2018**, *12*, 40−44.
(22) Melikyan, A.; Alloatti, L.; Muslija, A.; Hillerkuss, D.; Schindler, P. C.; Li, J.; Palmer, R.; Korn, D.; Muehlbrandt, S.; Van Thourhout, D.; Chen, B.; Dinu, R.; Sommer, M.; Koos, C.; Kohl, M.; Freude, W.; Leuthold, J. High-speed plasmonic phase modulators. *Nat. Photonics* **2014**, *8*, 229−233.
(23) Haffner, C.; Chelladurai, D.; Fedoryshyn, Y.; Josten, A.; Baeuerle, B.; Heni, W.; Watanabe, T.; Cui, T.; Cheng, B.; Saha, S.; Elder, D. L.; Dalton, L. R.; Boltasseva, A.; Shalaev, V. M.; Kinsey, N.; Leuthold, J. Low-loss plasmon-assisted electro-optic modulator. *Nature* **2018**, *556*, 483−486.
(24) Melikyan, A.; Kaneda, N.; Kim, K.; Baeyens, Y.; Dong, P. Differential drive I/Q modulator based on silicon photonic electro-absorption modulators. *J. Lightwave Technol.* **2020**, *38*, 2872−2876.
(25) Rao, A.; Patil, A.; Rabiei, P.; Honardoost, A.; DeSalvo, R.; Paolella, A.; Fathpour, S. High-performance and linear thin-film lithium niobate Mach−Zehnder modulators on silicon up to 50 GHz. *Opt. Lett.* **2016**, *41*, 5700−5703.
(26) Sun, S.; Xu, M.; He, M.; Gao, S.; Zhang, X.; Zhou, L.; Liu, L.; Yu, S.; Cai, X. Folded Heterogeneous Silicon and Lithium Niobate Mach−Zehnder Modulators with Low Drive Voltage. *Micromachines* **2021**, *12*, 823.
(27) Honardoost, A.; Juneghani, F. A.; Safian, R.; Fathpour, S. Towards subterahertz bandwidth ultracompact lithium niobate electrooptic modulators. *Opt. Express* **2019**, *27*, 6495−6501.
(28) Sun, S.; He, M.; Xu, M.; Zhang, X.; Ruan, Z.; Zhou, L.; Liu, L.; Liu, L.; Yu, S.; Cai, X. High-speed modulator with integrated termination resistor based on hybrid silicon and lithium niobate platform. *J. Lightwave Technol.* **2021**, *39*, 1108−1115.
(29) He, M.; Xu, M.; Ren, Y.; Jian, J.; Ruan, Z.; Xu, Y.; Gao, S.; Sun, S.; Wen, X.; Zhou, L.; Liu, L.; Guo, C.; Chen, H.; Yu, S.; Liu, L.; Cai, X. High-performance hybrid silicon and lithium niobate Mach−Zehnder modulators for 100 Gbit/s and beyond. *Nat. Photonics* **2019**, *13*, 359−364.
(30) Sun, S.; He, M.; Xu, M.; Gao, S.; Chen, Z.; Zhang, X.; Ruan, Z.; Wu, X.; Zhou, L.; Liu, L.; Lu, S.; Guo, X.; Liu, L.; Yu, S.; Cai, X. Bias-drift-free Mach−Zehnder modulators based on a heterogeneous silicon and lithium niobate platform. *Photonics Res.* **2020**, *8*, 1958−1963.
(31) Weigel, P. O.; Zhao, J.; Fang, K.; Al-Rubaye, H.; Trotter, D.; Hood, D.; Mudrick, J.; Dallo, C.; Pomerene, A. T.; Starbuck, A. L.; DeRose, C. T.; Lentine, A. L.; Rebeiz, G.; Mookherjea, S. Bonded thin film lithium niobate modulator on a silicon photonics platform exceeding 100 GHz 3-dB electrical modulation bandwidth. *Opt. Express* **2018**, *26*, 23728−23739.
(32) Wang, X.; Weigel, P. O.; Zhao, J.; Ruesing, M.; Mookherjea, S. Achieving beyond-100-GHz large-signal modulation bandwidth in hybrid silicon photonics Mach Zehnder modulators using thin film lithium niobate. *APL Photonics* **2019**, *4*, 096101.
(33) Weigel, P. O.; Valdez, F.; Zhao, J.; Li, H.; Mookherjea, S. Design of high-bandwidth, low-voltage and low-loss hybrid lithium niobate electro-optic modulators. *J. Phys.: Photonics* **2020**, *3*, 012001.
(34) Kharel, P.; Reimer, C.; Luke, K.; He, L.; Zhang, M. Breaking voltage−bandwidth limits in integrated lithium niobate modulators using micro-structured electrodes. *Optica* **2021**, *8*, 357−363.
(35) Xu, M.; Zhu, Y.; Pittalà, F.; Tang, J.; He, M.; Ng, W. C.; Wang, J.; Ruan, Z.; Tang, X.; Kuschnerov, M.; Liu, L.; Yu, S.; Zheng, B.; Cai, X. Dual-polarization thin-film lithium niobate in-phase quadrature modulators for terabit-per-second transmission. *Optica* **2022**, *9*, 61−62.
(36) Chen, G.; Chen, K.; Gan, R.; Ruan, Z.; Wang, Z.; Huang, P.; Lu, C.; Lau, A. P. T.; Dai, D.; Guo, C.; Liu, L. High performance thin-film lithium niobate modulator on a silicon substrate using periodic capacitively loaded traveling-wave electrode. *APL Photonics* **2022**, *7*, 026103.
(37) Wang, C.; Zhang, M.; Stern, B.; Lipson, M.; Lončar, M. Nanophotonic lithium niobate electro-optic modulators. *Opt. Express* **2018**, *26*, 1547−1555.
(38) Ghione, G. *Semiconductor Devices for High-Speed Optoelectronics*; Cambridge University Press, 2009.

https://doi.org/10.1021/acsphotonics.2c00263
ACS Photonics 2022, 9, 2668−2675

(39) Lv, J.; Yin, X.; Jin, J.; Zhang, H.; Zhao, C.; Peng, C.; Hu, W. Demonstration of a thermo-optic phase shifter by utilizing high-Q resonance in high-index-contrast grating. *Opt. Lett.* **2018**, *43*, 827−830.

Recommended by ACS

40 × 40 Metalens Array for Improved Silicon Photomultiplier Performance

Soh Uenoyama and Ryosuke Ota

MAY 21, 2021
ACS PHOTONICS

READ

Mode-Oriented Permutation Cipher Encryption and Passive Signal Switching Based on Multiobjective Optimized Silicon Subwavelength Metastructures

Hao Jia, Lin Yang, *et al.*

JULY 07, 2020
ACS PHOTONICS

READ

Si Microring Resonator Crossbar Array for On-Chip Inference and Training of the Optical Neural Network

Shuhei Ohno, Mitsuru Takenaka, *et al.*

JULY 22, 2022
ACS PHOTONICS

READ

Self-Configuring and Reconfigurable Silicon Photonic Signal Processor

Hailong Zhou, Xinliang Zhang, *et al.*

FEBRUARY 05, 2020
ACS PHOTONICS

READ

Get More Suggestions >

https://doi.org/10.1021/acsphotonics.2c00263
ACS Photonics 2022, 9, 2668−2675